Applied Catalysis B: Environmental 253 (2019) 187–195

Contents lists available at ScienceDirect

Applied Catalysis B: Environmental

journal homepage: www.elsevier.com/locate/apcatb

# Bi-modified Pt supported on carbon black as electro-oxidation catalyst for 300 W formic acid fuel cell stack

Mihwa Choi[a,b,1], Chi-Yeong Ahn[c,d,1], Hyunjoon Lee[c,d], Jong Kwan Kim[e], Seung-Hyeon Oh[e], Wonchan Hwang[c,d], Seugran Yang[a], Jungsuk Kim[a,b], Ok-Hee Kim[f], Insoo Choi[g], Yung-Eun Sung[c,d], Yong-Hun Cho[e,*], Choong Kyun Rhee[h,*], Woonsup Shin[b,*]

[a] New & Renewable Energy Laboratory, Korea Electric Power Corporation (KEPCO) Research Institute, Daejeon, 34056, Republic of Korea
[b] Department of Chemistry, Sogang University, Seoul, 04107, Republic of Korea
[c] Center for Nanoparticle Research, Institute for Basic Science (IBS), Seoul, 08826, Republic of Korea
[d] School of Chemical and Biological Engineering, Seoul National University, Seoul, 08826, Republic of Korea
[e] Department of Chemical Engineering, Kangwon National University, Samcheok, 25913, Republic of Korea
[f] Department of Science, Republic of Korea Naval Academy, Jinhae-gu, Changwon, 51704, Republic of Korea
[g] Division of Energy Engineering, Kangwon National University, Samcheok, 25913, Republic of Korea
[h] Department of Chemistry, Chungnam National University, Daejeon, 34134, Republic of Korea

ARTICLE INFO

*Keywords:*
Direct formic acid fuel cell
Irreversible Bi adsorption
Pt/C catalyst
MEA
Stack

ABSTRACT

Formic acid is a chemical with a simple molecular structure containing hydrogen. This liquid at room temperature is easy to handle and has a low toxicity, and is thus in the spotlight as a fuel. In particular, formic acid is an excellent fuel candidate because it can be operated at low temperatures when applied as a fuel in fuel cells with a high theoretical open-circuit voltage (1.48 V). However, it has a drawback in that the electrode catalyst is deactivated due to the generation of CO intermediates when formic acid is oxidized during cell operation. Therefore, to prevent this, an irreversibly adsorbed Bi on Pt catalyst is applied to a direct formic acid fuel cell (DFAFC) anode because it is easy to synthesize and economical. Physical analyses such as transmission electron microscopy (TEM), X-ray diffraction (XRD), and thermogravimetric analysis (TGA) were conducted, and electrochemical evaluations were performed through half-cell and single-cell level tests. The results revealed that the formic acid oxidation reaction activity of the Bi-modified Pt/C was 13 times higher than that of the conventional catalyst at 0.58 V. Further, a DFAFC stack was fabricated using the Bi-modified Pt/C, which yielded a power of 300 W. These results suggest that a simple synthesis method can be applied to fabricating industrially available DFAFC stacks.

## 1. Introduction

Polymer-based electrolyte fuel cells, such as a proton exchange membrane fuel cell (PEMFC), alkaline exchange membrane fuel cell (AEMFC), direct formic acid fuel cell (DFAFC), and direct methanol fuel cell (DMFC), are one of the attractive future energy sources owing to their low operating temperatures and high efficiencies [1,2]. With the development of technologies to convert carbon dioxide into formic acid for reduction of greenhouse gases, DFAFCs are receiving more attention [3–16]. As an energy storage medium, liquid formic acid can be conveniently transported and stored compared to hydrogen gas, which may explode in case of a minute leakage. For example, the use of liquid formic acid is advantageous in that it can be used as a fuel for power source devices in a mountainous area or a small island area where a city gas piping is difficult to install, and for power sources of portable devices or small-sized transportation vehicles. Formic acid has a low flammability, having a flash point of 69 °C, which is higher than those of other fuels like methanol (12 °C) or ethanol (16.6 °C), and its proton storage capacity by volume is 3.6 times that of compressed hydrogen at 350 bar [17]. In addition, it is less toxic and has lower crossover properties than methanol does in a fuel cell [18–22].

Formic acid oxidation on platinum (Pt) catalysts in DFAFCs occurs in two ways: direct reaction (dehydrogenation) and indirect reaction (dehydration) [23–26]. It is well known that CO intermediates produced in the indirect reaction pathway act as catalyst poisons and deteriorate the activity of Pt catalysts [27]. Direct reactions occur mainly

* Corresponding authors.
*E-mail addresses:* yhun00@gmail.com (Y.-H. Cho), ckrhee@cnu.ac.kr (C.K. Rhee), shinws@sogang.ac.kr (W. Shin).
[1] These authors contributed equally to this work

https://doi.org/10.1016/j.apcatb.2019.04.059
Received 6 September 2018; Received in revised form 31 March 2019; Accepted 18 April 2019
Available online 18 April 2019
0926-3373/ 

in the steps and terraces of Pt nanoparticles (NPs), while indirect reactions occur on plain Pt NPs [28]. However, since general Pt NPs have all these surface features, it is difficult to completely avoid the indirect reaction. Hence, new strategies are required to avoid indirect reactions. However, the preparation process of shape-controlled Pt NPs to increase the density of steps and terraces is complex, and thus, such Pt NPs are difficult to mass-produce. Therefore, to suppress the poisoning of the catalyst surface and to improve the performance of the fuel cells by a simple process, alloys of Pt or Pd with other metals such as Ni, Au, Bi, Pb, As, and Sb [29–43] or surface-modified catalysts [44–52] were investigated. Moreover, it has been reported that most Pt- or Pd-based alloy catalysts improve the performance of DFAFC compared to pure Pt or Pd. Particularly, the method of irreversibly adsorbing the second metal on the surface of the electrode, which is one of the strategies for surface modification of the catalyst, has become an important topic because it is a simple method in which oxygenated metal anions including oxides are strongly adsorbed on the electrode surface by immersing the electrode in the second metal's precursor solution [53].

Among the above-mentioned metal elements used for suppressing CO poisoning, Bi is known to greatly improve the electrocatalytic activity by geometrically separating adjacent Pt surface sites by the attachment of Bi adatoms to the surfaces of the Pt NPs [54–60]. Feliu and co-worker reported that Bi adatoms on tetrahexahedral Pt nanocrystals could contribute to the electronic effect by providing a third-body effect. They also explained that a higher Bi coverage increases the activity of formic acid and does not produce CO by dehydration of formic acid on the surface [61,62]. Kim et al. investigated the relationship between Bi coverage and formic acid oxidation in a catalyst, where Bi is irreversibly adsorbed on Pt NPs [63]. Further, Bi gives an ensemble effect, which enhances the dehydrogenation path and suppresses the dehydration path, and that the electronic effect is affected by the Pt thickness underneath the adsorbed Bi in previous report [64]. However, most of the above-mentioned studies focused only on the activity and poisoning of the catalyst, and studies on application to practical devices such as the DFAFC stacks is lacking.

In this study, the performance of the oxidizing catalyst was improved through the irreversible adsorption of Bi, and the feasibility of commercialization was confirmed by the optimized manufacturing process of a membrane electrode assembly (MEA). Electrochemical experiments were performed on a half-cell and single-cell using a catalyst in which Bi was irreversibly adsorbed on 40 wt% commercial Pt/C. The results demonstrate the excellent electro-oxidation performance of formic acid with Bi adatoms, and shows that the DFAFC performance could be greatly improved by a much smaller amount of Pt as compared with previous studies where a large amount of catalyst was used, as shown in Table 1 [23,65–67]. Furthermore, a stack of 35 MEAs was successfully fabricated, which yielded 300 W of power, and the strategy is expected to contribute to the commercialization of DFAFCs.

## 2. Experimental

### 2.1. Preparation of Bi-modified Pt supported on carbon black

$Bi_2O_3$ (99.999%, Sigma-Aldrich, USA) was added to 0.5 M $H_2SO_4$ (95–97%, Merck, Germany), and 40% Pt/C (Johnson Matthey, HiSPEC® 4000) was added to the solution. The mixture was stirred for 48 h to irreversibly adsorb $Bi^{3+}$ on the Pt surfaces. At this time, the amount of adsorbed Bi is controlled by the concentration of the $Bi^{3+}$ solution and the $Bi^{3+}$ concentration of the solution was 5 mM. After stirring, the remaining $Bi^{3+}$ ions in the solution were removed by washing with distilled water. A $NaBH_4$ solution was added to the washed catalyst, and the adsorbed $Bi^{3+}$ ions on the Pt NPs were reduced by stirring for 30 min. Then, it was washed several times with distilled water using a Buchner funnel-filtering apparatus (with a filter paper pore size of 2.5 μm) and finally dried in an oven at 60 °C for 3 h to obtain a Bi-modified Pt catalyst.

### 2.2. Physical characterization

The morphology of the prepared catalysts and the particle size of the catalysts were confirmed by TEM (Tecnai F20 at RIAM). In addition, the distribution of the irreversibly adsorbed Bi was confirmed by Cs-corrected high-resolution TEM (JEOL ARM200 F at KBSI) and energy dispersive X-ray spectroscopy (EDS, SDD type 80 T) using a high-angle annular dark-field scanning transmission electron microscope (HAADF-STEM). The crystal structure of the prepared Bi-modified Pt catalyst was analyzed by XRD (DMAX-2500 H) and the size of the NPs was calculated. The atomic ratio of the irreversibly adsorbed Bi was confirmed by inductively coupled plasma atomic emission spectroscopy (ICP-AES, OPTIMA 4300DV at NCIRF). Thermogravimetric analysis (TGA, TA Q600) was conducted to investigate the adsorption amount of Bi. To analyze the electronic state of the catalysts, X-ray photoelectron spectroscopy (XPS, SIGMA PROBE) was performed with an Al-Kα X-ray beam (1486.6 eV). The XPS peak deconvolution was obtained using the CasaXPS software. The Pt $4f_{7/2}$ and Pt $4f_{5/2}$ doublet was constrained to have a 4:3 integrated peak area ratio and an equal full width at half maximum (FWHM) value with a Shirley background. The fitting constraints for the peak area and FWHM of the Bi 4*f* were same as for Pt 4*f* [68]. The splitting values for Pt $4f_{7/2}$ - Pt $4f_{5/2}$ and Bi $4f_{7/2}$ - Bi $4f_{5/2}$ were 3.33 and 5.30 eV, respectively. The binding energies were calibrated with respect to C 1*s* at 285.0 eV.

### 2.3. Half-cell test

A saturated calomel electrode (SCE) was used as the reference electrode (RE), and a Pt mesh was used as the counter electrode (CE). As a working electrode, 5 μL of the prepared catalyst slurry was coated on a glassy carbon electrode (area 0.196 $cm^2$) to prepare a rotating disk electrode (RDE) wrapped in Teflon. The catalyst slurry was prepared by mixing the catalyst (5 mg) with 500 μL of isopropyl alcohol (IPA, Sigma-Aldrich) and 24.75 μL of 5% Nafion solution (Sigma-Aldrich) and dispersing in a sonic bath (Model 8510, Branson). The catalyst loadings were 0.1 $mg_{Pt}\,cm^{-2}$ in all half-cell tests. Cyclic voltammetry (CV) was performed using the RDE to analyze the hydrogen adsorption/desorption of the prepared Bi-modified Pt/C catalyst in the range of 0.05–1.05 V in 0.1 M $HClO_4$ solution. The oxygen reduction reaction (ORR) and hydrogen oxidation reaction (HOR) of the catalysts were measured in 0.1 M $HClO_4$ solution at a scan rate of 10 mV/s and an electrode rotation rate of 1600 rpm. To compare the catalytic activity of formic acid oxidation reaction (FAOR) of the catalysts, Ar-saturated 0.1 M $HClO_4$ with 0.5 M HCOOH aqueous solution was used at a scan rate of 50 mV/s in the range of 0.05–1.05 V. CO stripping [69] was

**Table 1**
Catalysts and performances of DFAFC single-cell electrodes reported in literature.

| Reference Number | Anode catalyst | Catalyst loading (mg $cm^{-2}$) | Cathode catalyst | Catalyst loading (mg $cm^{-2}$) | Maximum power density (mW $cm^{-2}$) |
|---|---|---|---|---|---|
| [23] | Pt Black | 4.0 | Pt Black | 7.0 | 48.8 |
| [65] | Pt Black | 4.0 | Pt Black | 7.0 | 119 |
| [66] | 60% PtRu/C | 3.0 $mg_{PtRu}\,cm^{-2}$ | Pt Black | 5.0 | 122 |
| [67] | 40% Pt-Au/C | 4.0 | 40% Pt/C | 4.0 | 184.8 |
| Our results | 40% Bi-modified Pt/C | 1.2 $mg_{PtBi}\,cm^{-2}$ | Pt Black | 3.0 | 191 |

conducted via linear sweep voltammetry (LSV) in a HCOOH-free 0.1 M $HClO_4$ solution (Ar saturated) at a scan rate of 10 mV/s from 0.05 to 1.2 V. Before CO stripping, electrodes were immersed in a 0.1 M $HClO_4$ solution containing 0.5 M HCOOH at an open circuit voltage (OCV) for 6 h.

### 2.4. Single-cell test and stack performance

MEAs were prepared by a catalyst-coated membrane (CCM) method for the PEMFC by directly spraying the anode and cathode layers on both sides of the membrane (NR212) using a manual air-brush system (GP2, Japan), and a catalyst-coated substrate (CCS) method in which the catalyst layer is coated by directly spraying the gas diffusion layers (GDLs) for the DFAFC, again using the manual air-brush system. The catalyst ink used for spraying was prepared by mixing 30 mg of the catalyst with 120 μL of deionized (DI) water, 130 μL of 5% Nafion solution, and 3 mL of isopropanol (IPA) (Sigma Aldrich). To verify the ORR performance, commercial 40% Pt/C (0.2 $mg_{Pt}\,cm^{-2}$) and the prepared catalyst (0.2 $mg_{BiPt}\,cm^{-2}$) were applied to the anode and cathode of the MEAs, respectively. Similarly, to confirm the HOR performance, the prepared catalyst (0.2 $mg_{BiPt}\,cm^{-2}$) and commercial 40% Pt/C (0.2 $mg_{Pt}\,cm^{-2}$) were applied to the anode and cathode, respectively. The GDL (JNTG-30-A3, JNTG) was assembled by placing both the anode and cathode sides. Hydrogen (150 ml $min^{-1}$) and air (800 ml $min^{-1}$) were supplied to the anode and cathode at a constant flow rate in a humidified state (70 °C, relative humidity (RH): 100%). For the FAOR activity, the catalyst ink for the anode was prepared by mixing 50 mg of the catalyst (Pt/C, Pt black, and Bi-modified Pt/C) with 500 μL of DI water, 50 mg of 5% Nafion solution, and 3.8 mL of IPA. In addition, the Pt black ink for the cathode was prepared by mixing 50 mg of the Pt black with 500 μL of DI water, 80 mg of 5% Nafion solution, and 1.6 mL of IPA. Bi-modified Pt/C (1.2 $mg_{BiPt}\,cm^{-2}$) and Pt black (3.0 $mg_{Pt}\,cm^{-2}$) were applied at the anode and cathode, respectively. The GDL was assembled by placing TGP-H-060 (Toray, Japan) and SGL 10BC (Sigracet, Germany) on the anode and cathode sides, respectively. The performance of the single cell was measured at 60 °C by supplying 6 M FA (5 ml $min^{-1}$) to the anode and humidified air (500 ml $min^{-1}$) to the cathode. For comparison, a commercial catalyst was applied to both the anode and cathode to fabricate a conventional MEA. The geometric electrode area of the MEAs used in all the single-cell tests was 5 $cm^2$. To fabricate the DFAFC stack, 35 MEAs with a geometric electrode area of 50 $cm^2$ were prepared using the manual air-brush system. Ten times as much catalyst ink as that used in the single-cell test was prepared. Bi-modified Pt/C (1.2 $mg_{BiPt}\,cm^{-2}$) and Pt black (3.0 $mg_{Pt}\,cm^{-2}$) were applied to the GDL for anode and cathode, respectively, and the solvents composed of 50 mg of Nafion solution with 166 mg of DI water and 420 μL of IPA (for anode) or 350 μL of 1-propanol (for cathode) were additionally sprayed to form the outer layer. Then MEAs with a N-117 membrane placed between the CCSs for the anode and cathode were hot-pressed at 140 °C with a pressure of 4 MPa for 5 min. The performance of the stack was measured at 60 °C by supplying 6 M FA (50 ml $min^{-1}$) to the anode and humidified air (5000 ml $min^{-1}$) to the cathode.

## 3. Results and discussion

### 3.1. Physical characterization

Fig. 1(a) is a schematic illustration that the surfaces of the Pt NPs are partially covered by irreversibly adsorbed Bi atoms. Since Bi ions ($Bi^{3+}$) are reduced after adsorption on the Pt surface in the solution, Bi atoms are formed in an irregularly shaped monolayer band; these adsorption patterns have been reported in previous studies [70]. The irreversibly adsorbed Bi monolayer consists of oxygenated species. The second layer can be deposited on the pristine layer; however, during the reduction process, it moves randomly into the voids, eventually forming an irregular monolayer. Fig. 1(b) and (c) show the TEM images of commercial Pt/C and the prepared catalyst, respectively. In both the cases, the metal catalyst is uniformly dispersed on the carbon support. Because Bi atoms exist as a single layer on the Pt surface, there is no significant difference in morphology. The average particle sizes, which were determined by counting 100 NPs on each catalyst, were 3.593 nm and 3.810 nm for the commercial Pt/C and Bi-modified Pt/C, respectively. Since Bi was partially adsorbed on the surface of the bulk Pt, the size of the metal particles slightly increased after the adsorption of Bi. HAADF-STEM was performed to confirm the distribution of Bi and Pt in the Bi-modified Pt/C, and the images are shown in Fig. 1(d). In addition, EDS mapping was conducted on the area enclosed by the white square box shown in Fig. 1(d), and the result is shown in Fig. 1(e–g). As expected, it is mainly consisted of Pt (green) surrounded by Bi (magenta). As previously reported [60], Bi atoms were dispersed on the Pt NP surface as monolayers and formed an irregular area.

The amount of adsorbed Bi was determined by TGA and is shown in Fig. 2(a). In both the catalysts, oxidation of the carbon support occurred at about 300 °C. After oxidation of the support, residual values of 38.9% and 43.6% were obtained for the commercial Pt/C and the prepared catalyst, respectively. This indicates that both the catalysts contain 38.9% of Pt, and 4.7% of Bi is adsorbed on the surface of Pt in the prepared catalyst (Bi/Pt ratio = 0.12). For detailed information on metal composition, ICP-AES analysis was conducted and the results are shown in Table 2 As expected, the catalysts are mostly composed of Pt (91.46%), with a small amount of Bi (8.54%) (Bi/Pt ratio = 0.093). The results obtained by TGA include the carbon support as well as the oxide formed on the metal surface because it was heated in an air atmosphere. On the other hand, since ICP-AES detects the metal itself, the result may be slightly different from the TGA result. XRD was conducted to determine the crystallinity and particle size of the metals in the catalysts using the Scherrer equation, and the results are shown in Fig. 2(b). In both the cases, mainly Pt peaks were observed. Depending on the element, the detection limit of XRD is known to range from 0.5–10 wt%. In the case of prepared catalyst, Bi was not detected in XRD analysis because the amount of Bi adsorbed on the Pt surface was less than 5 wt%. The average particle sizes of the calculated metal NPs are 3.026 nm and 3.103 nm for commercial Pt/C and the prepared catalyst, respectively. The particle sizes of the catalysts were slightly smaller than those obtained from the TEM analysis (Fig. 1), but showed a similar tendency. To obtain the surface information of the prepared catalyst, XPS analysis was carried out and the results are shown in Fig. 2(c) and (d). The Pt spectrum (Pt 4*f*) was composed of a doublet (Pt $4f_{7/2}$ and Pt $4f_{5/2}$) due to spin-orbit, while the peaks were deconvoluted into three components (Pt metal (orange), $Pt^{2+}$ in PtO (blue), and $Pt^{4+}$ in $PtO_2$ (green)). The Bi spectrum (Bi 4*f*) was also composed of a doublet (Bi $4f_{7/2}$ and Bi $4f_{5/2}$) with the peak deconvoluted into two components (Bi metal (orange) and $Bi^{3+}$ in $Bi_2O_3$ (blue). For commercial Pt/C, the relative proportions of Pt, PtO, and $PtO_2$ were 76.52%, 17.63%, and 5.85%, respectively (Fig. S1). Because the Pt NPs were exposed to air before the XPS measurement, a certain amount of oxide was present, even if nothing had been treated with this commercial catalyst. However, the proportion of Pt (74.30%) decreased and those of PtO (19.48%) and $PtO_2$ (6.22%) increased after the Bi adsorption, and the binding energy of Pt 4*f* slightly increased (˜0.1 eV) compared to that of Pt/C due to the interaction with Bi in the prepared catalyst. Unlike the results of Pt, a large difference was observed in the surface results of Bi. Bi 4*f* peaks, which were absent in the spectrum of conventional Pt/C, appeared in the spectrum of Bi-modified Pt/C. A small amount of adsorbed Bi was not detected in XRD; however, in XPS, information on the change in the binding energies of the Pt surface and adsorbed Bi were obtained. The proportions of Bi and $Bi^{3+}$ in $Bi_2O_3$ were 43.93% and 56.07%, respectively. The adsorbed $Bi^{3+}$ ions were reduced to metallic Bi with $NaBH_4$, but like the Pt NPs in commercial Pt/C described above, they appear to be partially oxidized by exposure to air before XPS measurement. Therefore, the above-mentioned analyses revealed that the

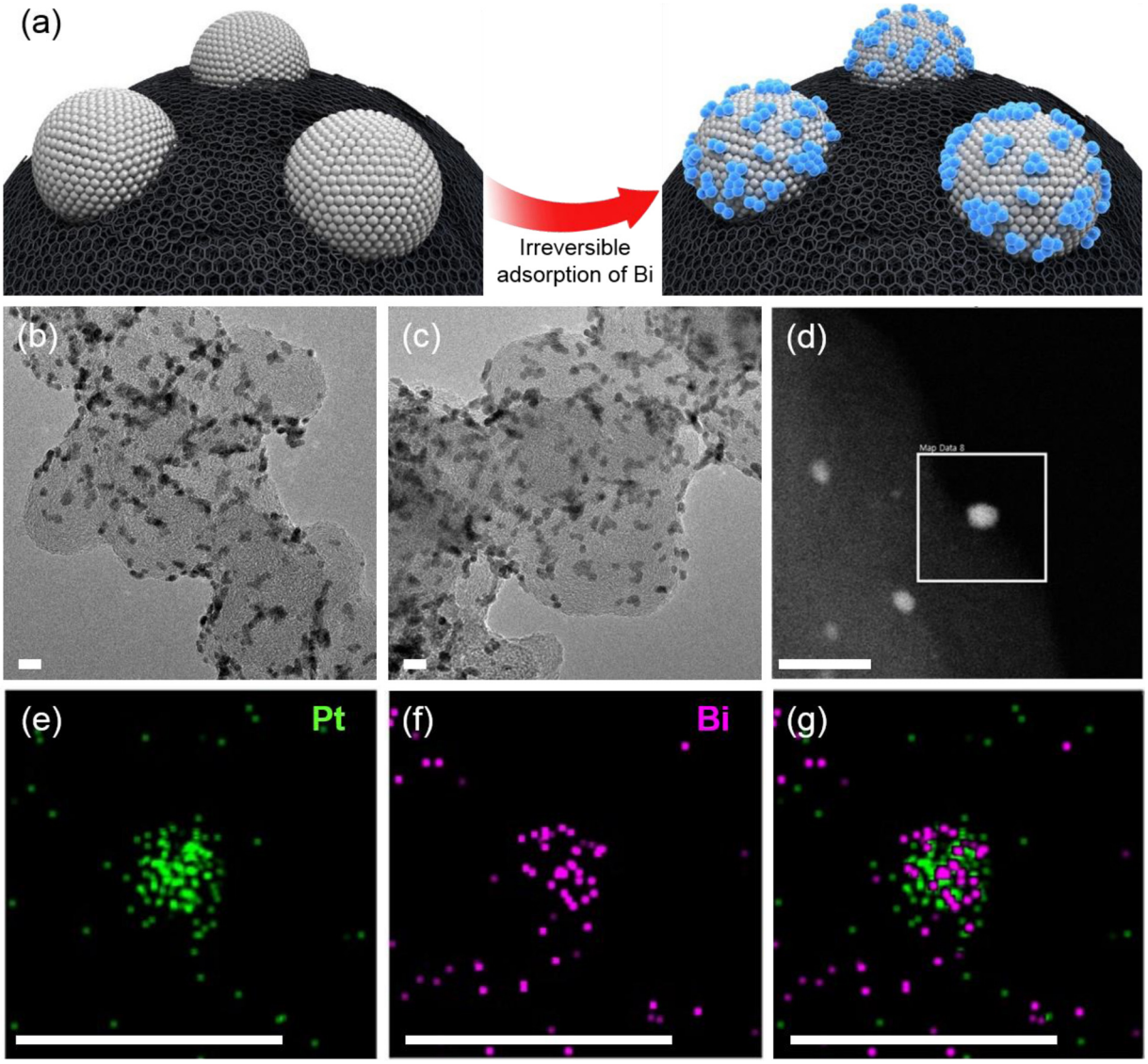


**Fig. 1.** Preparation of Bi-modified Pt/C. (a) Schematic diagram of adsorption of Bi on Pt/C. (b,c) TEM images of (b) commercial 40% Pt/C and (c) Bi-modified Pt/C. (d) HAADF-STEM image of Bi-modified Pt/C. (e–g) EDS maps of (e) Pt NP, (f) adsorbed Bi atoms, and (g) Pt and Bi. Scale bars are 10 nm.

amount of Bi adsorbed (including carbon support) on the Pt surface was less than 5 wt%, and that the adsorbed Bi influenced the electronic state of Pt in the prepared catalyst.

### 3.2. Electrochemical half-cell tests

To explore the electrochemical applicability of commercial Pt/C and Bi-modified Pt/C, half-cell tests were conducted under various conditions, and the results are shown in Fig. 3. For both the catalysts, CV was performed in $HClO_4$ solution (Fig. 3(a)). The area (charge, Q) of the hydrogen ($H_{upd}$) adsorption/desorption peaks of Bi-modified Pt/C from 0.05 to ~0.45 V was much smaller than the hydrogen adsorption/desorption peak area of Pt/C and it is also possible to calculate the electrochemical surface active area (ECSA) under half-cell conditions from this hydrogen charge. $H_{upd}$ due to the oxidation of $H_2$ is maximized in pure Pt/C, but is greatly reduced in the prepared catalyst due to the irreversibly adsorbed Bi on the Pt/C surface. The calculated ECSAs of the Pt/C and Bi-modified Pt/C are 79.34 $m^2 g^{-1}$ and 19.43 $m^2 g^{-1}$, respectively. In addition, the Bi coverage is a quantitative value of the amount of adsorbed Bi on the surface of the Pt NPs. The adsorption of Bi greatly inhibits the dehydration path of Pt/C, although, little amount of Bi cannot provide sufficient Pt ensembles, and too much Bi can block dehydrogenation Pt sites, or be oxidized itself at high voltage. Also, it is generally known that the coverage between 0.18 and 0.33 exhibits high FAOR activity [44,54,55]. Moreover, since three Pt atoms are blocked by one Bi atom theoretically, the coverage of Bi atoms on Pt nanoparticles can be calculated as follows: ($Q_{Pt/C}$,- $Q_{Bi\text{-}modified\ Pt/C}$)/(3$Q_{Pt/C}$) [63,71]. The Bi coverage calculated from the hydrogen charges is 0.25 which is proper value for high activity. Furthermore, an increase in the oxidation peaks was observed after the adsorption of Bi. Therefore, it was confirmed from the electrochemical CV results that Bi (coverage = 0.25) successfully adsorbed on the Pt surface. Fig. 3(b) shows the ORR results for the catalyst. After the adsorption of Bi on the catalyst surfaces, the on-set potential reduced and the half-wave potential negatively shifted from 0.92 V (Pt/C) to 0.86 V (Bi-modified Pt/C), which implies that the ORR performance of Bi-modified Pt/C is lower than that of conventional Pt/C. This is because although Pt is the best single metal for ORR activity, its active sites are blocked by the adsorbed Bi in the prepared catalyst. Fig. 3(c) shows the HOR activity of the Bi-adsorbed catalyst. Unlike ORR, a similar performance to that of conventional Pt/C was observed for HOR. HOR involving two electrons in the reaction is faster than ORR because of the presence of four electrons in the reaction and a large number of reaction intermediates. Therefore, it showed a high activity by Pt regardless of the adsorption of

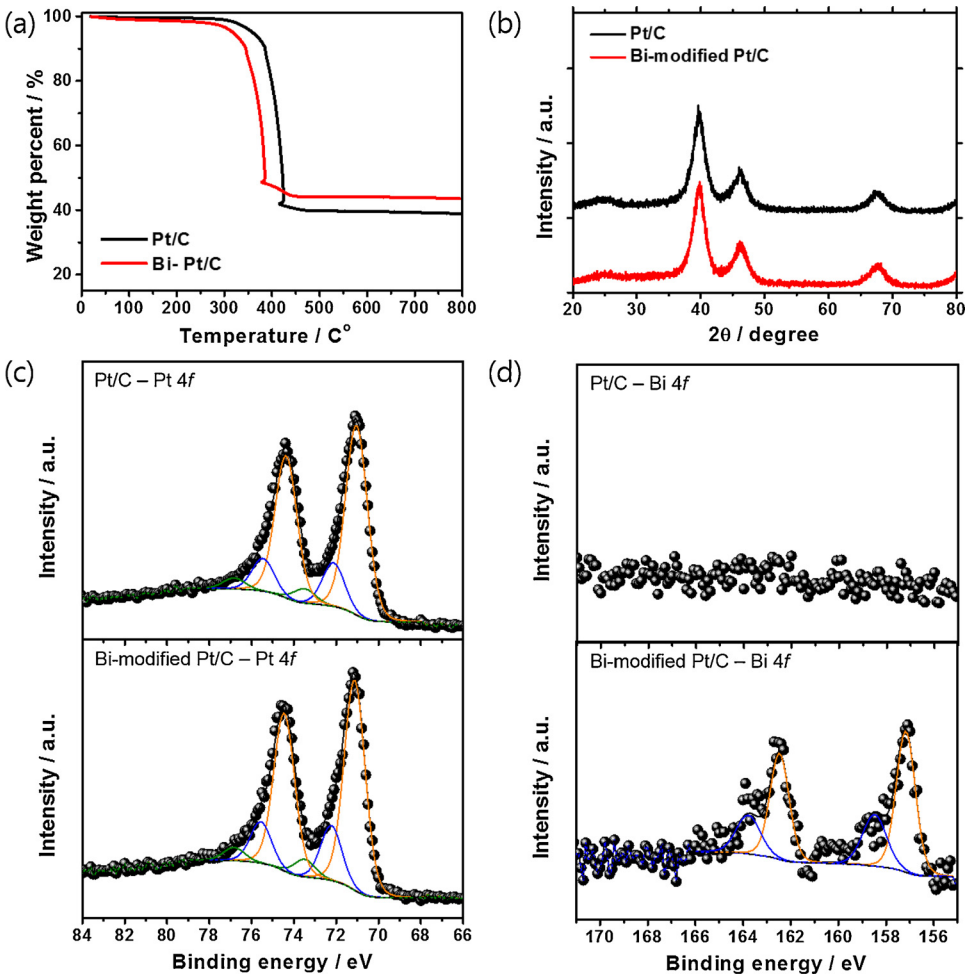


**Fig. 2.** Physical characteristics of the catalysts. (a) TGA profiles of Pt/C (black) and Bi-modified Pt/C (red). (b) XRD profiles of Pt/C (black) and Bi-modified Pt/C (red). (c) XPS spectra (Pt 4*f*) of Pt/C (top) and Bi-modified Pt/C (bottom). (d) XPS spectra (Bi 4*f*) of Pt/C (top) and Bi-modified Pt/C (bottom). (For interpretation of the references to colour in this figure legend, the reader is referred to the web version of this article).

Bi. In other words, Bi does not affect the HOR activity. Next, to obtain the FAOR activity, CV was performed in the presence of FA in the electrolyte, and the result is shown in Fig. 3(d). In the forward scan, a very small current density is observed in the case of conventional Pt/C, which indicates a low FAOR performance. A small and broad peak at ~0.58 V was observed, which is related to dehydrogenation. This is because Pt is poisoned by the CO intermediates formed when formic acid was oxidized via an indirect pathway. Therefore, FAOR hardly occurs on the passivated Pt surface, which results in a low current density. (A peak with a relatively large current density at ~0.98 V is a poison stripping peak.) On the other hand, in the case of Bi-modified Pt/C, the on-set potential (the potential at which a current of 1.89 mA $cm^{-2}$ is reached) of FAOR was less than 0.2 V, which was negatively shifted compared to Pt/C. At 0.58 V, the activity was ~13 times higher than that of the conventional catalyst. This evidences that the formation of poisoning CO intermediates is inhibited and that formic acid is oxidized through direct pathways. The adsorption of CO on Pt is a site demanding reaction [52]. However, because of the irreversible adsorption of Bi, the CO poisoning (indirect route of FAOR) is mostly inhibited. In other word, Bi does not act on the electrochemical catalysis itself, but acts as a third body because the direct route is promoted. Also, Bi enables the formation of Pt ensembles, and, therefore, it is considered that the desired FAOR reaction is selectively occurred in the presence of Bi adatoms. The turnover frequency (TOF) was derived from both the charge obtained in Fig. 3(a) and the dehydrogenation current at 0.58 V (Fig. 3(d)) of the two catalysts, as follows: ($j_{at\ 0.58\ V}$ $A_{electrode}$)/Q), where $j_{at\ 0.58\ V}$ and $A_{electrode}$ are the current density of the electrode at 0.58 V and the area of the electrode, respectively. The TOF of Bi-modified Pt/C (21,354 $h^{-1}$) was ~52 times higher than that of Pt/C (408 $h^{-1}$). The high TOF of Bi-modified Pt/C is due to the high electrochemical FAOR current, despite the low hydrogen charge of Pt. This high FAOR activity is because of the ensemble effect [63,64,70]. By the irreversible adsorption of Bi atoms, the surfaces of the Pt NPs are partially covered, as shown in Fig. 1(a). As a result, the Pt surface exposed to the electrolyte substantially decreases, and the Pt surface is only locally available for reaction. The exposed Pt forms a Pt ensemble, which is large enough for the direct path but too small for the indirect path for the oxidation of formic acid (ensemble effect). Therefore, the formation of poisoning CO intermediates was inhibited by the ensemble effect in Bi-modified Pt/C, and its FAOR activity was higher than that of conventional Pt/C. Additionally, as shown in Fig. 2c, the electronic interaction between the Bi and Pt may have made a small contribution to the catalytic activity [62]. Furthermore, CO stripping was performed to confirm the role of Bi adsorbed on the Pt surface as shown in Fig. S2. Since it was considered that the direct adsorption of CO gas on Pt NPs may be different from the adsorption of CO by the dissociation of HCOOH (formic acid), CO stripping using HCOOH solution was performed. The amount of CO oxidation can be determined from the integrated area of the peak, and the position of the stripping peak is an indicator of the ease of CO oxidation [38]. For example, a negative shift of the peak means that CO oxidation can easily occur on the surface of the catalyst, and a positive shift means the opposite. In the case of Bi-

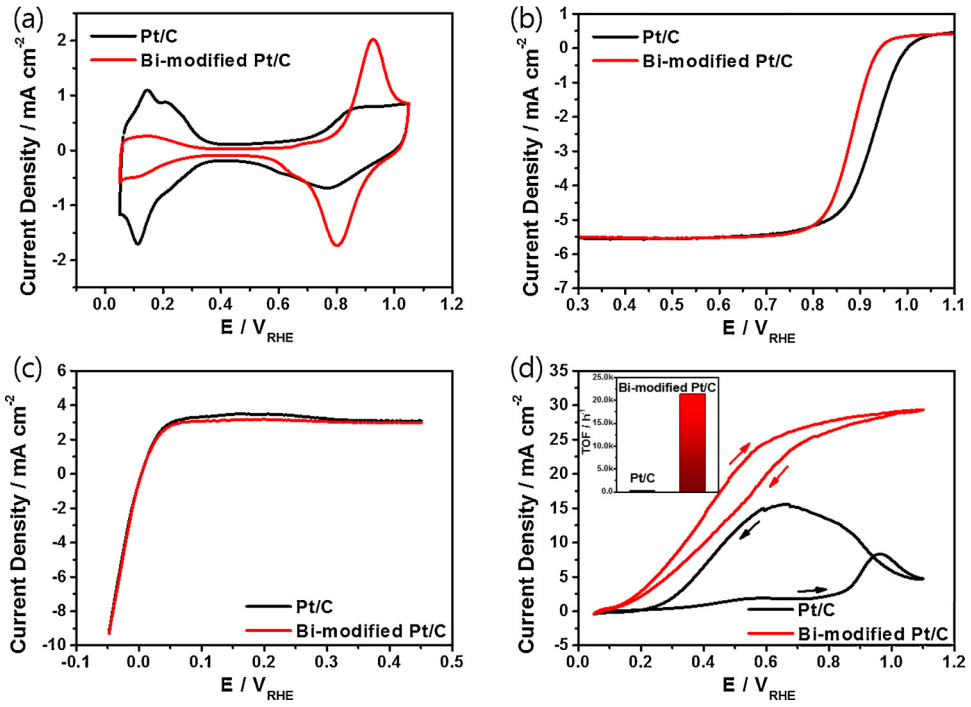


**Fig. 3.** Electrochemical half-cell tests. (a) CV, (b) ORR, (c) HOR, and (d) FAOR profiles (inset: TOFs) of Pt/C (black) and Bi-modified Pt/C (red) (For interpretation of the references to colour in this figure legend, the reader is referred to the web version of this article).

modified Pt/C, the area of CO was remarkably smaller than that in the case of Pt/C. However, the position of the peak of Bi-modified Pt/C (0.96 V) was positively shifted compared to that of Pt/C (˜0.77 V). This is an evidence that Bi blocks CO adsorption directly, rather than facilitating CO oxidation.

### 3.3. Single-cell and stack tests

Since the system configuration is simple compared to full cells (single-cell or stack), the half-cell is a suitable device for measuring the electrochemical performance of the catalyst because it can exclude other factors such as ohmic resistance or mass transfer. Although the full-cell system is complex and the preparation of MEA is difficult, it is important to measure the full-cell performance after manufacturing the MEA for practical applications of the fuel cell. This is because the electrochemical performance of an actual full cell is largely dependent on various parameters such as the anode, cathode, membrane, ionomer, and GDL, and the full cell includes a large current compared to the half-cell. Therefore, full-cell studies using MEAs are essential for practical applications and full commercialization of fuel cells. Fig. 4 shows the results of single-cell tests after manufacturing the MEAs. Similar to the results of the half-cell, although the same amount (0.2 mg cm$^{-2}$) of catalyst was applied to the MEAs, the ECSA calculated from the adsorption/desorption area of hydrogen (in the range of 0.05 ˜0.45 V) in the electrode comprising Bi-modified Pt/C was small (31.08 m g$^{-1}$) compared to that of the MEA with conventional Pt/C (51.62 m g$^{-1}$), as shown in Fig. 4(a). This is due to the adsorption of Bi, as described above in the half-cell results, and is an indirect evidence of successful Bi adsorption. To confirm the possibility of the prepared catalyst as an ORR catalyst, its performance was evaluated in $H_2$/air atmosphere and the result is shown in Fig. 4(b). Commercial Pt/C was applied to the anode in both the MEAs. The current density at 0.6 V was 27.1% lower than that of conventional MEA (reduced by 21.0% based on maximum power density). This appears to be an adverse effect of the adsorption of Bi on ORR activity in the cathode of the MEA. Fig. 4(c) shows the results obtained by applying the Pt/C catalyst (black) and the prepared catalyst (red) to the anode. For comparison, in both the cases, the cathode was prepared under the same conditions with commercial Pt/C. The maximum power density difference was only 2.4% between the MEA with Bi-modified Pt/C (653 mW cm$^{-2}$) and the conventional MEA (669 mW cm$^{-2}$). Besides, it showed almost the same electrochemical performance as that of the conventional MEA, even though another catalyst was applied to the anode of the MEA. As can be seen from the results of this experiment, even if the anode is changed while the cathode conditions are the same, there is little difference in the single-cell performances. This is because it is not the anode but the cathode that influences the overall performance of the fuel cell. Thus, when a catalyst with Bi is applied to an electrode (anode or cathode), the use of a common gaseous fuel ($H_2$ or $O_2$) causes a decrease in the performance of the fuel cell. However, Bi-modified Pt/C can play a role in the fuel cell where CO poisoning occurs due to the reaction intermediates, as confirmed in the half-cell studies. Therefore, the performance of the prepared catalyst for FAOR was confirmed in the MEA state, and the results are shown in Fig. 4(d). In this case, experiments were conducted on commercial Pt black NPs, commonly used for DFAFC anode, in addition to commercial Pt/C and Bi-modified Pt/C. Significant activation loss was observed in both the MEAs, except for the MEA with the prepared catalyst. The performance degradation is due to the adsorption of CO on the surface of Pt NPs due to the oxidation of the fuel (formic acid) through an indirect path. However, in the prepared catalyst with a small Pt ensemble formed by the partial adsorption of Bi atoms, CO generation was reduced, and thus, the performance of the MEA remarkably improved. The maximum power density of the MEA was 2.85 and 2.65 times higher than that of Pt/C and Pt black-applied MEA, respectively. In addition, the MEA exhibited a high voltage over the entire current density range, especially twice as high as that of the other two MEAs in the high current density region (340 mA cm$^{-2}$ at 0.5 V). This implies that when the same amount of current is needed in a fuel cell application, it maintains a higher voltage than the other MEAs do. Therefore, Bi-modified Pt/C, which demonstrated electrochemical applicability in the half-cell tests, was subjected to an actual fuel cell operating condition and exhibited an excellent performance in a DFAFC single cell.

To apply the MEA with Bi-modified Pt/C to practical fuel cells,

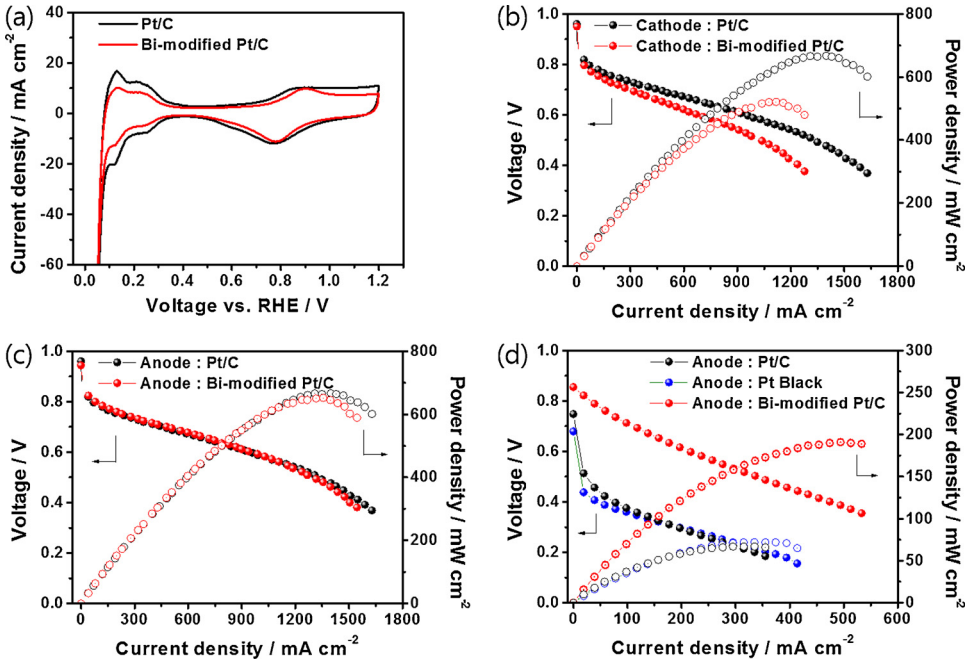


**Fig. 4.** Electrochemical evaluations of single cell with MEAs. (a) CV profiles measured in $N_2$ atmosphere. Performance curve of Bi-modified Pt/C applied to (b) cathode and (c) anode of the MEAs in air atmosphere. (d) Performance curves of DFAFC single cell with Pt/C (black), Pt black (blue), and Bi-modified Pt/C (red) applied to the anode (For interpretation of the references to colour in this figure legend, the reader is referred to the web version of this article).

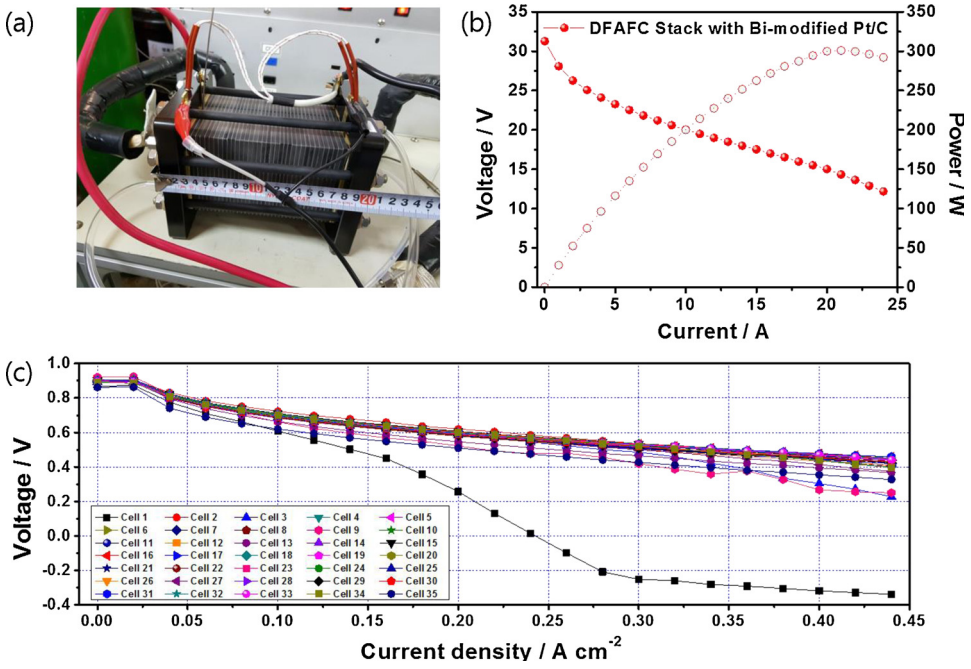


**Fig. 5.** DFAFC stack. (a) Detailed photo, (b) performance curve, and (c) individual MEA performance curves of the homemade DFAFC stack.

several MEAs were electrically connected to manufacture a fuel cell stack. When a fuel cell is used in an industrial field such as an automobile or a generator, most of it is applied in a stack to meet the voltage, current, or electric power requirements. Therefore, demonstrating and studying the performance of the stack is crucial for practical applications of the theoretical research results. As the number of MEAs increases, the voltage of the stack increases, and as the area increases, the output of the stack increases. Therefore, an enlarged MEA with Bi-modified Pt/C was prepared for the stack. Since the catalyst with Bi was prepared using an easy synthesis method (irreversible Bi adsorption) with the same quality, it was possible to increase the area of the MEA by using a decal transfer method easily. Thereafter, many identical MEAs were prepared to fabricate a DFAFC stack, and the relevant results are shown in Fig. 5. Fig. 5(a) shows a photograph of the fabricated DFAFC stack with Bi-modified Pt/C. The geometric area of each MEA is 50 $cm^2$, and 35 MEAs are stacked. The total dimension including the MEA, GDL, gasket, and bipolar plate (excluding the end plate) is 15.6 (width) × 11.6 (depth) × 9.8 (height) cm, and the total volume is about 1.76 L. The performance curve of the stack is shown in Fig. 5(b). OCV was measured above 31 V and no significant activation loss was observed in the low current region, similar to the performance of the single cell with Bi-modified Pt/C. Furthermore, the maximum power was 301 W. This is, as we know, the result of the stack showing the highest power with an electrode using a Pt-based catalyst in the DFAFC stack. To observe the behavior of each cell in the stack, the voltages were measured and the results are shown in Fig. 5(c). The cell was numbered from the point where the fuel was supplied, and the cell near the air inlet was named cell 35. In this case, no large activation loss was observed in all the

MEAs, and the performances of most cells were similar to that of the DFAFC single cell (Fig. 4(d)). However, relatively low performances were observed for cells 1, 2, and 3 compared with the other cells. This is because air was insufficiently supplied to the cell close to the anode, resulting in a low potential of the cell [72]. In particular, cell 1 showed a drastic decrease in performance at currents of 0.1 A $cm^{-2}$ or more, and even after 0.25 A $cm^{-2}$, a reverse voltage was observed. This seems to be caused by an insufficient supply of fuel to cell 1 [73]. As the anode potential increases due to fuel starvation, the total potential of the cell is reversed. The same results were observed when several tests were conducted. This is because the liquid fuel was not supplied to the anode of cell 1 due to the high flow rate, or probably due to the failure of the flow field design of the homemade cell. Overall, we have successfully manufactured a DFAFC stack with 300 W power by applying a Bi-modified Pt/C catalyst to the anode. Although low potentials have been observed in some cells, our ongoing research is likely to improve the performance through stack electrode optimization and cell design.

## 4. Conclusion

In this study, we have prepared a Bi-modified Pt/C catalyst by a simple and easy method. Physical analyses confirmed that Bi was irreversibly adsorbed on the surface of Pt. Furthermore, the electrochemical hydrogen adsorption/desorption results confirmed that the adsorbed Bi restricts the activity of Pt. Therefore, the ORR activity was lower than that of the conventional Pt/C. However, the FAOR activity of the prepared catalyst was 13 times higher than that of Pt/C. This is because most of the FAOR occurs through a direct route due to the adsorbed Bi as a third body which makes Pt ensembles, and thus, the generation of CO intermediates is significantly reduced. Further, the single-cell performance after MEA fabrication was improved when the prepared catalyst was applied to a DFAFC anode than when applied to a PEMFC anode and cathode. The MEA with Bi-modified Pt/C showed a power density of over 2.5 times that of the MEA with commercial catalysts (Pt/C and Pt black). The DFAFC stack was successfully manufactured by scale-up and duplicating 35 of the MEA, and 300 W of electric power was achieved on this stack. This achievement may provide the basis for the commercialization of DFAFCs.

## Declarations of interest

None

## Acknowledgements

This work was supported by Project Code IBS-R006-A2 and R14VF01 (Korea Electric Power Corporation) in Korea. This work was also supported by the Technology Development Program to Solve Climate Changes of the National Research Foundation (NRF) funded by the Ministry of Science and ICT (NRF-2018M1A2A2063172). Y.-H.C. acknowledges financial support from the Basic Science Research Program (2016R1D1A3B03934752) through the National Research Foundation of Korea (NRF), which is funded by the Ministry of Education.

## Appendix A. Supplementary data

Supplementary material related to this article can be found, in the online version, at doi:https://doi.org/10.1016/j.apcatb.2019.04.059.

## References

[1] K. Vignarooban, J. Lin, A. Arvay, S. Kolli, I. Kruusenberg, K. Tammeveski, L. Munukutla, A.M. Kannan, Nano-electrocatalyst materials for low temperature fuel cells: a review, Chinese J. Catal. 36 (2015) 458–472.
[2] N. Rajalakshmi, J.R. Imran, K.S. Dhathathreyan, Research advancements in Low-temperature fuel cells, in: M. Thandavarayan, V.S. Saji (Eds.), Electrocatalysts for Low Temperature Fuel Cells, Wiley-VCH Verlag GmbH & Co, KGaA, 2017.
[3] S. Enthaler, J. von Langermann, T. Schmidt, Carbon dioxide and formic acid—the couple for environmental-friendly hydrogen storage? Synth. Lect. Energy Environ. Technol. Sci. Soc. 3 (2010) 1207–1217.
[4] Y.-P. Peng, Y.-T. Yeh, S.I. Shah, C.P. Huang, Concurrent photoelectrochemical reduction of $CO_2$ and oxidation of methyl orange using nitrogen-doped $TiO_2$, Appl. Catal. B: Environ. 123-124 (2012) 414–423.
[5] H.-R.M. Jhong, S. Ma, P.J.A. Kenis, Electrochemical conversion of $CO_2$ to useful chemicals: current status, remaining challenges, and future opportunities, Current Opin. Chem. Eng. 2 (2013) 191–199.
[6] G. Qin, Y. Zhang, X. Ke, X. Tong, Z. Sun, M. Liang, et al., Photocatalytic reduction of carbon dioxide to formic acid, formaldehyde, and methanol using dye-sensitized $TiO_2$ film, Appl. Catal. B: Environ. 129 (2013) 599–605.
[7] L. Lyu, X. Zeng, J. Yun, F. Wei, F. Jin, No catalyst addition and highly efficient dissociation of H2O for the reduction of $CO_2$ to formic acid with Mn, Environ. Sci. Tech. 48 (2014) 6003–6009.
[8] D.H. Won, C.H. Choi, J. Chung, S.I. Woo, Photoelectrochemical production of formic acid and methanol from carbon dioxide on metal-decorated CuO/$Cu_2O$-layered thin films under visible light irradiation, Appl. Catal. B: Environ. 158-159 (2014) 217–223.
[9] S. Zhang, P. Kang, T.J. Meyer, Nanostructured tin catalysts for selective electrochemical reduction of Carbon Dioxide to formate, J. Am. Chem. Soc. 136 (2014) 1734–1737.
[10] T. Baran, S. Wojtyła, A. Dibenedetto, M. Aresta, W. Macyk, Zinc sulfide functionalized with ruthenium nanoparticles for photocatalytic reduction of $CO_2$, Appl. Catal. B: Environ. 178 (2015) 170–176.
[11] R. Kortlever, I. Peters, S. Koper, M.T.M. Koper, Electrochemical $CO_2$ reduction to formic acid at Low Overpotential and with high faradaic efficiency on carbon-supported bimetallic Pd–Pt nanoparticles, ACS Catal. 5 (2015) 3916–3923.
[12] F. Yoshitomi, K. Sekizawa, K. Maeda, O. Ishitani, Selective formic acid production via $CO_2$ reduction with visible light using a hybrid of a perovskite tantalum oxynitride and a binuclear ruthenium(II) complex, ACS Appl. Mater. Interfaces 7 (2015) 13092–13097.
[13] Z. Bitar, A. Fecant, E. Trela-Baudot, S. Chardon-Noblat, D. Pasquier, Electrocatalytic reduction of carbon dioxide on indium coated gas diffusion electrodes—comparison with indium foil, Appl. Catal. B: Environ. 189 (2016) 172–180.
[14] D.B. Kayan, F. Köleli, Simultaneous electrocatalytic reduction of dinitrogen and carbon dioxide on conducting polymer electrodes, Appl. Catal. B: Environ. 181 (2016) 88–93.
[15] T. Su, H. Tian, Z. Qin, H. Ji, Preparation and characterization of Cu modified $BiYO_3$ for carbon dioxide reduction to formic acid, Appl. Catal. B: Environ. 202 (2017) 364–373.
[16] X. Wang, X. Zhao, D. Zhang, G. Li, H. Li, Microwave irradiation induced UIO-66-$NH_2$ anchored on graphene with high activity for photocatalytic reduction of $CO_2$, Appl. Catal. B: Environ. 228 (2018) 47–53.
[17] J. Eppinger, K.-W. Huang, Formic acid as a hydrogen energy carrier, ACS Energ. Letters 2 (2017) 188–195.
[18] Y.-W. Rhee, S.Y. Ha, R.I. Masel, Crossover of formic acid through Nafion® membranes, J. Power Sources 117 (2003) 35–38.
[19] X. Wang, J.-M. Hu, I.M. Hsing, Electrochemical investigation of formic acid electrooxidation and its crossover through a Nafion® membrane, J. Electroanal. Chem. Lausanne (Lausanne) 562 (2004) 73–80.
[20] C.M. Miesse, W.S. Jung, K.-J. Jeong, J.K. Lee, J. Lee, J. Han, S.P. Yoon, S.W. Nam, T.-H. Lim, S.-A. Hong, Direct formic acid fuel cell portable power system for the operation of a laptop computer, J. Power Sources 162 (2006) 532–540.
[21] S.Z. Rejal, M.S. Masdar, S.K. Kamarudin, A parametric study of the direct formic acid fuel cell (DFAFC) performance and fuel crossover, Inter. J. Hydrogen Energ. 39 (2014) 10267–10274.
[22] S. Ha, R. Larsen, Y. Zhu, R.I. Masel, Direct Formic Acid Fuel Cells with 600 mA $cm^{-2}$ at 0.4 V and 22 °C, Fuel Cells Weinh. (Weinh) 4 (2004) 337–343.
[23] C. Rice, S. Ha, R.I. Masel, P. Waszczuk, A. Wieckowski, T. Barnard, Direct formic acid fuel cells, J. Power Sources 111 (2002) 83–89.
[24] J.D. Lović, A.V. Tripković, S.L. Gojković, K.D. Popović, D.V. Tripković, P. Olszewski, A. Kowal, Kinetic study of formic acid oxidation on carbon-supported platinum electrocatalyst, J. Electroanal. Chem. Lausanne (Lausanne) 581 (2005) 294–302.
[25] X. Yu, P.G. Pickup, Recent advances in direct formic acid fuel cells (DFAFC), J. Power Sources 182 (2008) 124–132.
[26] W. Gao, J.A. Keith, J. Anton, T. Jacob, Theoretical elucidation of the competitive electro-oxidation mechanisms of formic acid on Pt(111), J. Am. Chem. Soc. 132 (2010) 18377–18385.
[27] S. Uhm, H.J. Lee, J. Lee, Understanding underlying processes in formic acid fuel cells, Phys. Chem. Chem. Phys. 11 (2009) 9326–9336.
[28] C. Jung, T. Zhang, B.-J. Kim, J. Kim, C.K. Rhee, T.-H. Lim, Formic acid oxidation on Bi-modified Pt nanoparticles of various sizes, Bull. Korean Chem. Soc. 31 (2010) 1543–1550.
[29] J.L. Haan, K.M. Stafford, R.I. Masel, Effects of the addition of Antimony, tin, and lead to palladium catalyst formulations for the direct formic acid fuel cell, J. Phys. Chem. C. 114 (2010) 11665–11672.
[30] Tu Dandan, B. Wu, B. Wang, C. Deng, Y. Gao, A highly active carbon-supported PdSn catalyst for formic acid electrooxidation, Appl. Catal. B: Environ. 103 (2011) 163–168.
[31] M. Ren, Y. Kang, W. He, Z. Zou, X. Xue, D.L. Akins, H. Yang, S. Feng, Origin of performance degradation of palladium-based direct formic acid fuel cells, Appl. Catal. B: Environ. 104 (2011) 49–53.

[32] X. Yu, P.G. Pickup, Screening of PdM and PtM catalysts in a multi-anode direct formic acid fuel cell, J. Appl. Electrochem. 41 (2011) 589–597.
[33] J. Shim, J. Lee, Y. Ye, J. Hwang, S.-K. Kim, T.-H. Lim, U. Wiesner, J. Lee, One-pot synthesis of intermetallic electrocatalysts in ordered, large-pore mesoporous Carbon/Silica toward formic acid oxidation, ACS Nano 6 (2012) 6870–6881.
[34] L. Shen, H. Li, L. Lu, Y. Luo, Y. Tang, Y. Chen, T. Lu, Improvement and mechanism of electrocatalytic performance of Pd–Ni/C anodic catalyst in direct formic acid fuel cell, Electrochim. Acta 89 (2013) 497–502.
[35] K. Jiang, W.-B. Cai, Carbon supported Pd-Pt-Cu nanocatalysts for formic acid electrooxidation: synthetic screening and componential functions, Appl. Catal. B: Environ. 147 (2014) 185–192.
[36] D. Wu, M. Cao, M. Shen, R. Cao, Sub-5 nm Pd–Ru nanoparticle alloys as efficient catalysts for formic acid electrooxidation, ChemCatChem 6 (2014) 1731–1736.
[37] T. Maiyalagan, X. Wang, A. Manthiram, Highly active Pd and Pd–Au nanoparticles supported on functionalized graphene nanoplatelets for enhanced formic acid oxidation, RSC Adv. 4 (2014) 4028–4033.
[38] A.M. Mohammad, G.A. El-Nagar, I.M. Al-Akraa, M.S. El-Deab, B.E. El-Anadouli, Towards improving the catalytic activity and stability of platinum-based anodes in direct formic acid fuel cells, Inter. J. Hydrogen Energ. 40 (2015) 7808–7816.
[39] S. Hu, F. Munoz, J. Noborikawa, J. Haan, L. Scudiero, S. Ha, Carbon supported Pd-based bimetallic and trimetallic catalyst for formic acid electrochemical oxidation, Appl. Catal. B: Environ. 180 (2016) 758–765.
[40] X. Jiang, X. Yan, W. Ren, Y. Jia, J. Chen, D. Sun, L. Xu, Y. Tang, Porous AgPt@Pt nanooctahedra as an efficient catalyst toward formic acid oxidation with predominant dehydrogenation pathway, ACS Appl. Mater. Interfaces 8 (2016) 31076–31082.
[41] A.K. Singh, S. Singh, A. Kumar, Hydrogen energy future with formic acid: a renewable chemical hydrogen storage system, Catal. Sci. Tech. 6 (2016) 12–40.
[42] T. Szumełda, A. Drelinkiewicz, E. Lalik, R. Kosydar, D. Duraczyńska, J. Gurgul, Carbon-supported $Pd_{100-X}Au_X$alloy nanoparticles for the electrocatalytic oxidation of formic acid: Influence of metal particles composition on activity enhancement, Appl. Catal. B: Environ. 221 (2018) 393–405.
[43] J. Zhang, M. Chen, H. Li, Y. Li, J. Ye, Z. Cao, M. Fang, Q. Kuang, J. Zheng, Z. Xie, Stable palladium hydride as a superior anode electrocatalyst for direct formic acid fuel cells, Nano Energ. 44 (2018) 127–134.
[44] M. Watanabe, M. Horiuchi, S. Motoo, Electrocatalysis by ad-atoms: part XXIII. Design of platinum ad-electrodes for formic acid fuel cells with ad-atoms of the IVth and the Vth groups, J. Electroanal. Chem. Interfacial Electrochem. 250 (1988) 117–125.
[45] B. Peng, J.-Y. Wang, H.-X. Zhang, Y.-H. Lin, W.-B. Cai, A versatile electroless approach to controlled modification of Sb on Pt surfaces towards efficient electrocatalysis of formic acid, Electrochem. commun. 11 (2009) 831–833.
[46] X. Yu, P.G. Pickup, Pb and Sb modified Pt/C catalysts for direct formic acid fuel cells, Electrochim. Acta 55 (2010) 7354–7361.
[47] B. Peng, H.-F. Wang, Z.-P. Liu, W.-B. Cai, Combined surface-enhanced infrared spectroscopy and first-principles study on electro-oxidation of formic acid at Sb-Modified Pt electrodes, J. Phys. Chem. C. 114 (2010) 3102–3107.
[48] J.-Y. Wang, Y.-Y. Kang, H. Yang, W.-B. Cai, Boron-doped palladium nanoparticles on carbon black as a superior catalyst for formic acid electro-oxidation, J. Phys. Chem. C. 113 (2009) 8366–8372.
[49] F. Si, J. Ge, C. Li, L. Liang, C. Liu, W. Xing, Investigations of Pt modified Pd/C catalyst synthesized by one-pot galvanic replacement for formic acid electro-oxidation, Inter. J. Hydrogen Energ. 39 (2014) 2489–2496.
[50] A. Ferre-Vilaplana, J.Vc. Perales-Rondón, J.M. Feliu, E. Herrero, Understanding the effect of the adatoms in the formic acid oxidation mechanism on Pt(111) electrodes, ACS Catal. 5 (2015) 645–654.
[51] M. Bełtowska-Brzezinska, T. Łuczak, J. Stelmach, R. Holze, The electrooxidation mechanism of formic acid on platinum and on lead ad-atoms modified platinum studied with the kinetic isotope effect, J. Power Sources 251 (2014) 30–37.
[52] T.J. Schmidt, R.J. Behm, B.N. Grgur, N.M. Markovic, P.N. Ross, Formic acid oxidation on pure and Bi-Modified Pt(111): temperature effects, Langmuir 16 (2000) 8159–8166.
[53] J. Kim, C.K. Rhee, Structural evolution of irreversibly adsorbed Bi on Pt(111) under potential excursion, J. Solid State Electrochem. 17 (2013) 3109–3114.
[54] J. Clavilier, A. Fernandez-Vega, J.M. Feliu, A. Aldaz, Heterogeneous electrocatalysis on well defined platinum surfaces modified by controlled amounts of irreversibly adsorbed adatoms: part I. Formic acid oxidation on the Pt (111)-Bi system, J. Electroanal. Chem. and Inter. Electrochem 258 (1989) 89–100.
[55] M.D. Maciá, E. Herrero, J.M. Feliu, A. Aldaz, Formic acid self-poisoning on bismuth-modified stepped electrodes, J. Electroanal. Chem. Lausanne (Lausanne) 500 (2001) 498–509.
[56] A. López-Cudero, F.J. Vidal-Iglesias, J. Solla-Gullón, E. Herrero, A. Aldaz, J.M. Feliu, Formic acid electrooxidation on Bi-modified Pt(110) single crystal electrodes, J. Electroanal. Chem. Lausanne (Lausanne) 637 (2009) 63–71.
[57] V. Grozovski, V. Climent, E. Herrero, J.M. Feliu, Intrinsic activity and poisoning rate for HCOOH oxidation on platinum stepped surfaces, Phys. Chem. Chem. Phys. 12 (2010) 8822–8831.
[58] V. Pautienienė, L. Tamašauskaitė-Tamašiūnaitė, A. Sudavičius, G. Stalnionis, Z. Jusys, Spontaneous Bi-modification of polycrystalline Pt electrode: fabrication, characterization, and performance in formic acid electrooxidation, J. Solid State Electrochem. 14 (2010) 1675–1680.
[59] J. Kim, C.K. Rhee, Ensemble size estimation in formic acid oxidation on Bi-modified Pt(111), Electrochem. commun. 12 (2010) 1731–1733.
[60] A. Sáez, E. Expósito, J. Solla-Gullón, V. Montiel, A. Aldaz, Bismuth-modified carbon supported Pt nanoparticles as electrocatalysts for direct formic acid fuel cells, Electrochim. Acta 63 (2012) 105–111.
[61] E. Leiva, T. Iwasita, E. Herrero, J.M. Feliu, Effect of adatoms in the electrocatalysis of HCOOH oxidation, A Theoretical Model. Langmuir 13 (1997) 6287–6293.
[62] Q.-S. Chen, Z.-Y. Zhou, F.J. Vidal-Iglesias, J. Solla-Gullón, J.M. Feliu, S.-G. Sun, Significantly enhancing catalytic activity of tetrahexahedral Pt nanocrystals by Bi adatom decoration, J. Am. Chem. Soc. 133 (2011) 12930–12933.
[63] B.-J. Kim, K. Kwon, C.K. Rhee, J. Han, T.-H. Lim, Modification of Pt nanoelectrodes dispersed on carbon support using irreversible adsorption of Bi to enhance formic acid oxidation, Electrochim. Acta 53 (2008) 7744–7750.
[64] J.K. Yoo, C.K. Rhee, Formic acid oxidation on Bi-modified Pt surfaces: Pt deposits on Au versus bulk Pt, Electrochim. Acta 216 (2016) 16–23.
[65] S. Ha, C.A. Rice, R.I. Masel, A. Wieckowski, Methanol conditioning for improved performance of formic acid fuel cells, J. Power Sources 112 (2002) 655–659.
[66] B. Fang, M. Kim, J.-S. Yu, Hollow core/mesoporous shell carbon as a highly efficient catalyst support in direct formic acid fuel cell, Appl. Catal. B: Environ. 84 (2008) 100–105.
[67] C. Venkateswara Rao, C.R. Cabrera, Y. Ishikawa, Graphene-supported Pt–Au alloy nanoparticles: a highly efficient anode for direct formic acid fuel cells, J. Phys. Chem. C. 115 (2011) 21963–21970.
[68] G.A. El-Nagar, M.A. Hassan, I. Lauermann, C. Roth, Efficient direct formic acid fuel cells (DFAFCs) anode derived from seafood waste: migration mechanism, Sci. Rep. 7 (2017) 17818.
[69] G.A. El-Nagar, M.S. El-Deab, A.M. Mohammad, B.E. El-Anadouli, Promoting effect of hydrocarbon impurities on the electro-oxidation of formic acid at Pt nanoparticles modified GC electrodes, Electrochim. Acta 180 (2015) 268–279.
[70] J.K. Yoo, M. Choi, S. Yang, B. Shong, H.-S. Chung, Y. Sohn, C.K. Rhee, Formic acid electrooxidation activity of Pt and Pt/Au catalysts: effects of surface physical properties and irreversible adsorption of Bi, Electrochim. Acta 273 (2018) 307–317.
[71] N. Furuya, S. Motoo, Arrangement of ad-atoms of various kinds on substrates: part I. Platinum substrate, J. Electroanal. Chem. Interfacial Electrochem. 98 (1979) 189–194.
[72] M. Dou, M. Hou, D. Liang, Q. Shen, H. Zhang, W. Lu, Z. Shao, B. Yi, Behaviors of proton exchange membrane fuel cells under oxidant starvation, J. Power Sources 196 (2011) 2759–2762.
[73] J. Kang, D.W. Jung, S. Park, J.-H. Lee, J. Ko, J. Kim, Accelerated test analysis of reversal potential caused by fuel starvation during PEMFCs operation, Int. J. Hydrogen Energ. 35 (2010) 3727–3735.